

Phase sensitive topological classification of single-qubit measurements in linear cluster states

Sougata Bhattacharyya^{1,*} and Sovik Roy ^{1,2,3,†}

¹*Dept. of Astronomy, Astrophysics and Space Engineering,
Indian Institute of Technology, Indore 453552, India*

²*Dept. of Mathematics, Techno Main Salt Lake (Engg. Colg.),
Techno India Group, EM 4/1, Sector V, Salt Lake, Kolkata 700091, India*

³*Centre of Advanced Studies and Innovation Lab (CASILAB),
18/27 Kali Mohan Road, Tarapur, Silchar 788003, INDIA*

We provide an explicit geometric classification of single-qubit projective measurements on one-dimensional linear cluster states within a topological framework. By establishing an explicit geometrical correspondence between local measurements and topological surgery operations on an associated link model i.e. a *measurement–surgery correspondence*, we represent the cluster state as a linear Hopf chain. Within this model, measurements in the computational (Z) basis act as *topological severance* in case of bulk measurements while *boundary pruning* happens for end measurements of qubits. In contrast, transverse (X) basis measurements remove the measured qubit while splicing its neighbours, preserving connectivity through real-valued correlations. We show that lateral (Y) basis measurements also preserve connectivity but generate intrinsically complex phase factors that are not captured by unframed link models, rendering X and Y measurements topologically indistinguishable at the level of connectivity alone. To resolve this ambiguity, we introduce a *framed ribbon representation* in which quantum phases are encoded as geometric twists, with *chiral $\pm 90^\circ$ twists* corresponding to the phases $\pm i$. This framing yields a phase-sensitive and outcome-resolved topological description of all single-qubit measurements on linear cluster states. Our approach provides a unified geometric interpretation of measurement-induced entanglement transformations in measurement-based quantum computation, revealing that quantum phases correspond directly to framed topological invariants. The work is restricted to one-dimensional linear cluster states and single-qubit measurements in the Pauli bases.

PACS numbers: 03.67.Lx, 03.67.Pp, 03.65.Vf, 03.65.Ud

Keywords: Measurement-Based Quantum Computation; Cluster States; Topological Quantum Information; Knot Theory; Framed Ribbons; Quantum Measurements; Entanglement Topology; Quantum Phases

I. INTRODUCTION

Measurement-Based Quantum Computation (MBQC) is also known as one-way quantum computing (OQC) as the computation proceeds in a single irreversible direction driven entirely by measurements. It constitutes an alternative paradigm for quantum information processing (QIP) in which computation is implemented solely through local measurements performed on a highly entangled many-body resource states [1, 2]. In this framework, entanglement is consumed rather than generated during computation, and the logical evolution is encoded in the adaptive choice of measurement bases together with classical feedforward of outcomes. Classical feedforward in QIP is a control strategy where measurement outcomes from one part of a quantum system are used to deterministically select and apply correction operations to another part of the system [3–6].

A canonical resource for MBQC is the cluster state, a highly entangled quantum state of multiple qubits

arranged in a lattice or graph structure [1, 3, 9, 10, 12]. These states are prepared by initializing qubits in the $|+\rangle$ state and applying Controlled-Z (CZ) or (a specific type of Controlled phase gate) gates between nearest neighbours, following the pattern of a graph where vertices represent qubits and edges represent entanglement [4, 12, 13]. While the stabilizer formalism and measurement calculus provide a complete algorithmic framework for describing measurements on graph states via graph transformations and Pauli by-products [3–6, 10, 11, 14, 15], they offer limited physical insights into the consequent restructuring of entanglement, especially when measurements introduce complex phases.

We posit that the underlying dynamics of measurements, particularly the emergence of complex phases, are inherently geometric phenomena. These may be characterized not merely through graph-theoretic updates, but through the evolution of the state's intrinsic topological structure. Topological methods have proven valuable in diverse areas of quantum theory, including topological quantum computation [16–18], knot invariants in quantum field theory [19], and the geometric classification of quantum phases [20–26]. Qualitative analogies between multipartite entanglement and linked/knotted structures have been explored [27, 28], establishing knot theory

* msc2503121011@iiti.ac.in

† s.roy2.tmsl@ticollege.org

as a promising language for describing nonlocal correlations and their phase reorganization. However, a precise operational correspondence between quantum measurements and topological surgery has not been systematically established. Recently, we undertook a series of studies investigating the role of topology and measurement-induced phases in quantum systems, emphasizing structural features that go beyond stabilizer and graph-theoretic updates [29, 30].

While the measurement calculus and stabilizer graph-transformation rules already provide a complete algebraic description of measurement effects on cluster states, these frameworks do not offer a phase-sensitive geometric representation of measurement-induced correlations. In particular, conventional link based topological analogies capture connectivity changes but remain insensitive to complex phase structure. The principal contribution of the present work is to introduce a frame topological representation in which measurement-induced quantum phases are encoded geometrically as ribbon twists, yielding a phase resolved topological description of single-qubit measurements on linear cluster states (LCS) [1, 2, 5, 31, 32].

In this work, we develop a phase-sensitive framed-topological representation that provides a geometric classification of single-qubit projective measurements on one-dimensional (1D) LCS. By establishing an explicit isomorphism between local measurement choices and topological surgery operations on an associated link model, we introduce the *measurement-cutting correspondence*. Within this framework, the 1D linear cluster state is represented by a linear Hopf chain, in which each qubit corresponds to a closed loop and each nearest neighbour CZ interaction is encoded as a Hopf link. We emphasize on two types of measurements viz. bulk-qubit measurements and end-qubit measurements of LCS. With respect to the structure of N -qubits LCS that would be defined in later sections, (i) a bulk-qubit measurement refers to measuring a qubit located inside the chain ($1 < k < N$) that has two neighbours and (ii) an end-qubit measurement refers to measuring a qubit located at the boundary of linear cluster (e.g. Q_1 or Q_N) which has only one neighbour.

We show that projective measurement in the computational (Z) basis corresponds to a topological cutting operation that removes the measured component and, for measurements in the bulk qubits, disconnects the chain into independent segments. We call this as *topological severance* or simply *severance*. On the other hand, the end-qubit measurements yield *unlinking* the terminal ring.

In contrast, measurement in the transverse (X) basis induces a *topological splicing* operation, whereby the measured component is removed while its neighbouring components are fused, thereby preserving connectivity

through real-valued correlations. These constructions furnish a direct geometric representation of the standard graph state measurement update rules.

A central result of our present work, however, concerns measurements performed in the lateral (Y) basis. While Y -basis measurements preserve connectivity in the same manner as X -basis measurements, they generate intrinsically complex phase factors of $\pm i$ that are not captured within conventional unframed link models. As a consequence, X and Y measurement outcomes become *topologically indistinguishable* when *connectivity alone is considered*, revealing a fundamental ambiguity in unframed topological representations. To resolve this issue, we introduce a *framed ribbon representation*, drawing on the mathematical theory of framed knots [28, 34], in which quantum correlations are encoded not only through connectivity but also via geometric twist. Within this extended framework, real-valued correlations correspond to untwisted or orientation-flipped ribbons, while complex phases are represented by *chiral* $\pm 90^\circ$ *twists*. This mapping from quantum phase to geometric torsion (a quantity that measures how a curve or framed object twists out of a plane as it propagates in space) parallels the correspondence between quantum evolution and geometric phases [23, 33], and yields a complete, phase-sensitive topological description of all single-qubit projective measurements on the LCS. The present results should therefore be viewed as a geometric reformulation of known measurement update rules, augmented by a new phase sensitive framed-topological structure that encodes measurement-induced Pauli frame corrections.

Taken together, our results establish a unified geometric framework for understanding measurement-induced entanglement transformations in MBQC. Beyond providing conceptual clarity, the framed topological model offers a systematic method for visualizing by-product operators, distinguishing measurement outcomes, and tracking the flow of quantum information. The approach naturally extends to higher-dimensional cluster states and suggests an essential role for framed topology in the characterization of phase-sensitive quantum correlations, potentially offering new insights into fault-tolerant quantum computation and the geometric classification of quantum resources.

The remainder of this paper is organized as follows. Sec. *II* introduces the foundational concepts required for the analysis, including projective quantum measurements, Schmidt rank based entanglement characterization, and essential notions from knot and link topology. In Sec. *III* we define the one-dimensional linear cluster state and establish the notation used throughout the work. Sec. *IV* develops the operational topological framework by introducing the measurement surgery correspondence and the linear Hopf chain representation of cluster states. Secs. *V* and *VI* analyze the topological effects of single-qubit mea-

surements in the Z , X , and Y bases, respectively, highlighting the connectivity preserving and phase-generating distinctions between measurement classes. Sec. *VII* summarizes the mathematical outcomes of all measurement scenarios, while Sec. *VIII* discusses the topological ambiguity between X and Y basis measurements in conventional link representations. Sec. *IX* introduces the framed ribbon model that resolves this ambiguity through a phase-sensitive topological description, and Sec. *X* applies this framework to classify measurement-induced transformations in detail. Finally, Sec. *XI* concludes with implications of the proposed geometric framework and directions for future research.

II. FOUNDATIONAL CONCEPTS

II.1. Quantum Projective Operations

A projective quantum operation is characterized by an *observable*, represented by a Hermitian operator \mathcal{M} acting on the Hilbert space of the system. This operator admits a spectral resolution $\mathcal{M} = \sum_m m P_m$, where the eigenvalues m correspond to distinct measurement outcomes, and each P_m is the orthogonal projector onto the eigenspace associated with m . These projectors satisfy Hermiticity $P_m = P_m^\dagger$, idempotence $P_m^2 = P_m$, and the completeness relation $\sum_m P_m = I$ [35].

For a tripartite quantum state $|\psi_{ABC}\rangle$, a projective measurement performed exclusively on subsystem A in its standard basis $\{|0\rangle, |1\rangle\}$ is defined by the set of operators P_k^A with $k = 0, 1$, where $P_k^A = |k\rangle_A \langle k| \otimes I_B \otimes I_C$. According to the Born rule, the probability of recording outcome k is

$$p(k) = \langle \psi_{ABC} | P_k^A | \psi_{ABC} \rangle. \quad (1)$$

Conditioned on this outcome, the physical state of the remaining subsystems B and C collapses to the post-measurement state

$$|\psi_{BC}^{(k)}\rangle = \frac{P_k^A |\psi_{ABC}\rangle}{\sqrt{p(k)}}. \quad (2)$$

The entanglement characteristics of this resultant bipartite state $|\psi_{BC}^{(k)}\rangle$ form the central object of our investigation.

II.2. The Schmidt Rank and Entanglement Quantification

For any pure bipartite state $|\psi_{BC}\rangle$ shared between parties B and C , there exists a canonical representation known as the Schmidt decomposition [36] given as

$$|\psi_{BC}\rangle = \sum_{i=1}^R \sqrt{\lambda_i} |\phi_B^i\rangle \otimes |\chi_C^i\rangle, \quad (3)$$

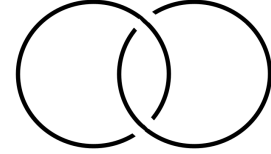


Figure 1: The Hopf link

where the sets $|\phi_B^i\rangle$ and $|\chi_C^i\rangle$ constitute orthonormal bases for the respective subsystems. The coefficients λ_i are non-negative real numbers satisfying $\sum_i \lambda_i = 1$, and the integer R denotes the *Schmidt rank*. The Schmidt rank serves as a fundamental discrete measure of bipartite entanglement [35, 36]. Thus we have,

- If $R = 1$, the state is separable, representing a simple product state with no entanglement.
- If $R > 1$, the state is entangled. The specific distribution of the λ_i further quantifies the degree of entanglement.
- A state with $R = 2$ and $\lambda_1 = \lambda_2 = \frac{1}{2}$ corresponds to a maximally entangled bipartite state, such as a Bell pair.

In our protocol, we compute the Schmidt rank of the conditional state $|\psi_{BC}^{(k)}\rangle$ to classify the entanglement status between qubits B and C following the local measurement on the qubit A .

II.3. Topology of Links and Knots

Knot theory provides a mathematical framework for studying the embedding of closed curves within three-dimensional space. A *knot* is defined as a single, non-self-intersecting closed loop, considered non-trivial if it cannot be smoothly deformed into a simple circle (the *unknot*). A *link* generalizes this concept to a collection of one or more such knots, which may be interwoven [34]. Two links are deemed topologically equivalent if one can be continuously transformed into the other without any cutting or piercing of strands. The topological analogue to a local quantum measurement is the *deletion* of a single link component.

II.4. The Hopf Link

The *Hopf link* (See Fig. 1) is the minimal non-trivial link comprising of two circles. Its defining feature is that each circle is linked with the other. If one component is cut and removed, the remaining component becomes a trivial *unknot*, representing a state of complete *unlinking* [34].

III. THE LINEAR CLUSTER STATE

III.1. Definition

The N -qubit linear cluster state $|C_N\rangle$ is a specific instance of a graph state corresponding to a 1D line graph. It is canonically defined by initializing a register of N qubits in the product state $|+\rangle^{\otimes N}$ and applying a Controlled-Phase (CZ) gate between all adjacent pairs $(i, i+1)$, where the suffix i denote the i^{th} qubit of the state. Explicitly, the state can be written in the computational basis as

$$|C_N\rangle = \frac{1}{2^{N/2}} \sum_{x_1, \dots, x_N \in \{0,1\}} (-1)^{\sum_{i=1}^{N-1} x_i x_{i+1}} |x_1 \dots x_N\rangle, \quad (4)$$

where the exponent $\sum_{i=1}^{N-1} x_i x_{i+1}$ encodes the phase correlations characteristic of the 1D Ising interaction. 1D Ising interaction refers to a nearest neighbour two qubit interaction whose phase structure is mathematically identical to the interaction term in the 1D Ising model. In the classical (where spins take classical values $s_i = \pm 1$) or in the quantum (where spins are represented by quantum operators such as Pauli matrices) Ising model, the interaction energy between neighbouring spins i and $i+1$ is proportional to $\sigma_z^{(i)} \sigma_z^{(i+1)}$ is nearest neighbours along a 1D chain. In LCS, qubits produce phase factors $(-1)^{x_i x_{i+1}}$ which has the same mathematical structure as the Ising nearest neighbour coupling term. Thus, the cluster state phase pattern can be viewed as arising from an effective 1D Ising type interaction between adjacent qubits.

The LCS state defined in Eq.(4), possesses maximal connectedness and persistent entanglement, making it the universal resource for OQC [9, 37]. For our further topological analysis of the state, we shall use notation such as $|C_L\rangle$ and $|C_R\rangle$ which are the left and right segments of cluster state $|C_N\rangle$ in the following sections.

IV. OPERATIONAL TOPOLOGY: THE MEASUREMENT-CUTTING CORRESPONDENCE

To rigorously classify the measurement dynamics of the cluster state, we adopt an operational-topological framework that bridges quantum information theory with knot theory. In this paradigm, the abstract algebraic process of quantum measurement is mapped directly to a concrete geometric operation called *Topological Surgery*.

IV.1. The Isomorphism

The fundamental correspondence relies on the *destructive nature* of projective measurement. When a qubit within an entangled system is measured in a standard basis, it is

projected onto a product state, effectively disentangling it from the rest of the wavefunction.

- *Quantum Operation*: A local projective measurement $\mathcal{M}_{\text{proj}}$ on qubit Q_k collapses the superposition, factoring the global state $|\Psi\rangle$ into a product of the measured qubit and the residual system i.e. $|\phi\rangle_k \otimes |\Psi'\rangle_{\text{rest}}$. Consequently, the qubit Q_k ceases to be a resource for entanglement.
- *Topological Analogue*: This corresponds to the physical CUTTING (OR DELETION) of the ring k from the topological chain. The ring is removed from the manifold, and the stability of the remaining structure depends entirely on how the surviving end-points are connected.

Thus, we define the mapping as

$$\mathcal{M}_{\text{proj}}^{(k)} \iff \text{Topological Component Deletion (Cut } k\text{)} \quad (5)$$

IV.2. Measurement as a Stress Test

This isomorphism allows us to treat quantum measurement as a *topological stress test*. By mathematically performing the measurement and analyzing the residual state, we can determine the connectivity of the underlying topology. However, the LCS exhibits a richer phenomenology than simple binary connectivity. While the *Cut* is the fundamental operation for all measurements, the *basis* of the measurement (Z , X , or Y) *imposes different boundary conditions* on the surgery. These conditions determine whether the cut-ends (a) remain severed, (b) are fused back together, or (c) acquire additional geometric structure. Accordingly, distinguishing the topological effects of different measurement bases requires examining not only whether the chain remains connected but also *how* the geometry of the link is modified by the operation.

IV.3. The Topological Analogy: Linear Hopf Chain

We propose a direct topological visualization for the 1D LCS $|C_N\rangle$ of Eq. (4), which we refer to as the *Linear Hopf Chain*, drawing inspiration from earlier topological approaches to quantum entanglement [27, 28]. Rather than viewing the state purely as an abstract graph, we map the quantum resource onto a *physical assembly of interlocked components*.

In this framework, the quantum correlations are translated into topological constraints as follows:

- *Qubits as Topological Loops*: We view each physical qubit Q_i as a distinct and closed topological ring.

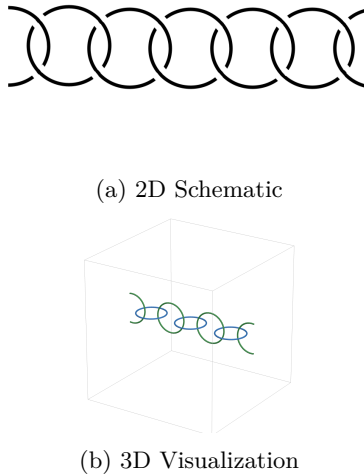


Figure 2: **The Linear Hopf Chain Model.** (a) 2D diagrammatic representation of the 1D cluster state connectivity. (b) 3D visualization of the same state as a series of physically interlinked rings. In this dual picture, quantum measurements correspond to topological operations (cutting or splicing) performed on these links.

- *Interactions as Hopf Links:* The entanglement bond between two neighbouring qubits is represented physically as a HOPF LINK. The two rings pass through each other exactly once, establishing a robust connection (as shown in Fig. 1).
- *Linear Connectivity:* The strictly local nature of the cluster state means that only adjacent rings are linked. Distant rings do not interact, resulting in a linear chain-like topology.

This model provides a concrete interpretation of the quantum system, as visualized in Fig. 2.

The *flow of information* along the cluster state is *isomorphic* to the *mechanical connectivity* of the chain. Consequently, a local measurement on a qubit is topologically equivalent to *cutting* and *removing* that specific ring from the assembly.

V. THE Z AND X-BASIS MEASUREMENTS:

We begin by analyzing projective measurements on the LCS in the Z and X bases.

V.1. Topological Cutting

The simplest operation in the measurement calculus is the projection onto the computational basis, $\mathcal{M}_Z = \{|0\rangle, |1\rangle\}$.

While transverse (X basis) and lateral (Y basis) measurements reshape the entanglement connectivity, the Z -basis measurement is fundamentally destructive. We classify this operation as a *Topological Cut*. This operation serves as the baseline for the topological surgery. In the topological picture, a Z -basis measurement acts like a cutting operation, i.e., the qubit is projected out of the entangled state and effectively removed from the connectivity graph. By performing this removal, one can observe how the remaining structure changes (e.g. whether the chain splits), thereby revealing the role that node played in maintaining the connectivity. We analyze this dynamic in two distinct regimes viz. the severing of internal links (Bulk) and the shortening of the chain (End).

V.1.1. Internal Severance (Bulk Measurement)

Mathematically, measuring a bulk qubit k ($1 < k < N$) in the Z -basis disentangles it entirely from the graph state. As derived explicitly in APPENDIX A.3, the post-measurement state factorizes into a tensor product of two independent cluster states as shown below.

$$|\Psi_{\text{final}}\rangle = \sigma_{\text{bound}} (|C_L\rangle_{1\dots k-1} \otimes |C_R\rangle_{k+1\dots N}), \quad (6)$$

where σ_{bound} represents the Pauli Z byproduct operators $Z_{k-1}Z_{k+1}$ that arise only for the outcome $|1\rangle_k$ (Pauli Z byproduct operators are outcome-dependent Pauli Z corrections that arise on the remaining qubits following a projective measurement and can be compensated by classical feedforward operations.) Crucially, the Schmidt Rank R across the partition collapses to unity (i.e. $R = 1$), indicating a total loss of quantum correlations between the left (C_L) and right (C_R) segments.

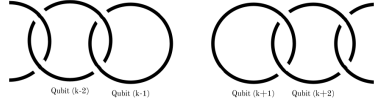
Topologically, this maps to the physical removal of the central ring k from the Hopf chain, as illustrated in Fig. 3. Unlike the Splicing operations (X and Y) which fuse neighbours, the Z measurement deletes the bridge.

V.1.2. Boundary Pruning (End Measurement)

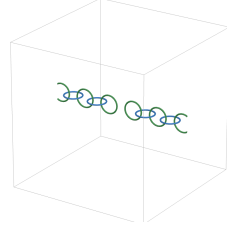
When the measurement targets an end-point qubit ($k = 1$), the topology is not severed into two, but rather *shortened*. As shown in APPENDIX A.2. Measuring qubit 1 yields a residual state on the remaining $N - 1$ qubits.

$$|\Psi_{\text{final}}\rangle = \sigma_2^\mu |C_{N-1}\rangle_{2\dots N}, \quad (7)$$

where σ_2^μ denotes an outcome dependent Pauli operator ($\mu \in \{0, x, y, z\}$ such that $\sigma^0 = I$, $\sigma^x = X$, $\sigma^y = Y$ and $\sigma^z = Z$) acting on qubit 2 with identity operating on all other qubits.



(a) Bulk Measurement (2D Schematic)



(b) Bulk Measurement (3D Visualization)

Figure 3: Topological Cutting in the Z-Basis - Internal Severance. Measuring a bulk qubit (Q_k) physically removes the central ring. Unlike Splicing (which fuses neighbours), Severance destroys the path, leaving two unlinked, independent segments ($R = 1$).

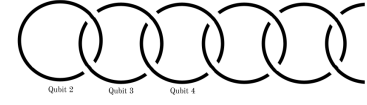
Topologically, this corresponds to unlinking and discarding the terminal ring. The chain remains continuous but is reduced in length by one unit ($N \rightarrow N - 1$). Unlike an X -basis measurement, which can shift the effective computational boundary forward by propagating information along the chain, a Z -basis measurement merely removes the terminal qubit without further altering the connectivity; we refer to this operation as *topological pruning*, depicted in Fig. 4.

V.2. Topological Splicing

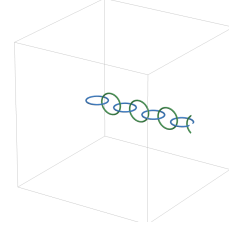
While the Z -basis measurement acts as a destructive *Severance*, breaking the quantum channel, the transverse (X) basis measurement, $\mathcal{M}_X = \{|+\rangle, |-\rangle\}$, performs a fundamentally constructive operation which we classify as *Topological Splicing*. This contrast is central to MBQC where Z removes connectivity to shape the logic, X preserves connectivity to propagate information.

V.3. Internal Splicing (Bulk Measurement)

Considering a projective measurement of a bulk-qubit Q_k , ($1 < k < N$) in the transverse basis $\mathcal{M}_X = \{|+\rangle, |-\rangle\}$, we see that unlike Z basis measurement, which removes the qubit and breaks the entanglement chain, an X -basis measurement removes the physical site (i.e. lattice vertex correspondence to qubit Q_k) while preserving global connectivity through a measurement induced fusion of its



(a) End Measurement (2D Schematic)



(b) End Measurement (3D Visualization)

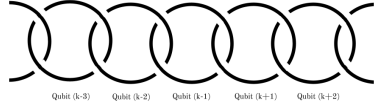
Figure 4: Topological Cutting in the Z -Basis - Boundary Pruning. Measuring an end qubit (Q_1) removes the terminal ring. The chain remains connected but shortens ($N \rightarrow N - 1$). Contrast this with X -basis propagation, shown in Fig. 6: here, the boundary moves only one step, to Q_2 .

nearest neighbours $k - 1$ and $k + 1$. The resulting post measurement state can be written as

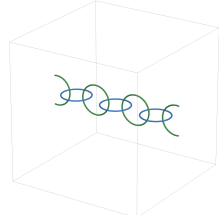
$$|\Psi_{\text{final}}\rangle = \sigma_{k-1}^{\mu} |C_{N-1}^{(k-1 \leftrightarrow k+1)}\rangle, \quad (8)$$

where $\mu \in \{0, z\}$ labels the outcome dependent Pauli by-product operator acting on qubit Q_{k-1} (with $\sigma^0 = I$ and $\sigma^z = Z$). The notation $k - 1 \leftrightarrow k + 1$ denotes the graph update induced by the measurement - the measured vertex k is deleted and a new entangling edge is created directly between its former neighbours $k - 1$ and $k + 1$. Consequently, the resulting state $|C_{N-1}^{(k-1 \leftrightarrow k+1)}\rangle$ is a cluster state on $N - 1$ qubits whose adjacency structure is identical to the original linear chain except that the intermediate vertex k has been removed and replaced by a direct bond between the neighbouring sites. Across the bipartition separating the left and right segments of the chain, the Schmidt rank $R = 2$, confirming that the measurement implements topological splicing rather than the severance. In the Hopf chain representation, the removal of ring Q_k is accompanied by the creation of a direct Hopf link between rings Q_{k-1} and Q_{k+1} , thereby maintaining a continuous entanglement path along the chain.

Throughout the paper, the notation $i \leftrightarrow j$ denoted the measurement-induced insertion of a direct entangling edge between vertices i and j after deletion of the measured vertex.



(a) Bulk Measurement (2D Schematic)



(b) Bulk Measurement (3D Visualization)

Figure 5: Topological Splicing in X-Basis - Internal Splicing. The critical contrast to Z-severance. Measuring Q_k fuses the neighbors Q_{k-1} and Q_{k+1} into a direct link, preserving the linear topology ($R = 2$) instead of breaking it.

V.4. Boundary Propagation (End Measurement)

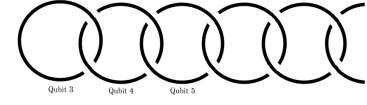
The contrast extends to the boundary i.e. the difference between Z -basis and X -basis measurement effects, already observed for bulk-qubits, also appears when the measured qubit lies at the edge of the chain. A Z -measurement on end-qubit 1 simply shortens the chain by one unit ($N \rightarrow N - 1$). However, an X -measurement on end-qubit 1 triggers a *skipping* effect. As shown in APPENDIX B.1, the measurement effectively disentangles the *next* qubit (Q_2), forcing it into a fixed computational state (typically $|0\rangle$). The active boundary of the cluster effectively jumps to Q_3

$$|\Psi_{\text{final}}\rangle \approx |0\rangle_2 \otimes |C_{N-2}\rangle_{3\dots N} \quad (9)$$

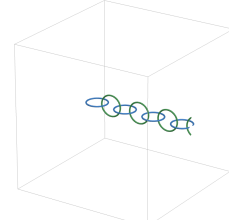
This demonstrates the information propagation capability of the X -basis, visualized in Fig. 6. Unlike the passive Z -pruning, the X -splice actively pushes the logical information forward along the chain.

VI. THE Y-BASIS MEASUREMENT: LIMITS OF THE STANDARD TOPOLOGICAL MODEL

Finally, we address the measurement in the lateral basis, $\mathcal{M}_Y = \{|+i\rangle, |-i\rangle\}$. This operation presents a unique structural challenge that highlights the fundamental limitations of standard graph-state visualizations.



(a) End Measurement (2D Schematic)



(b) End Measurement (3D Visualization)

Figure 6: Topological Splicing in X-Basis - Boundary Propagation. Unlike Z -pruning, measuring Q_1 in X decouples Q_2 , effectively transporting the boundary to Q_3 .

VI.1. Internal Connectivity (Bulk Measurement)

Mathematically, measuring a bulk-qubit k in the Y -basis preserves the entanglement chain. As derived in APPENDIX C.2, this operation removes site k (or qubit k), but fuses the neighbours $k - 1$ and $k + 1$ into a connected state. The residual wave function is

$$|\Psi_{\text{final}}\rangle = (S_{k-1}^\mu \otimes S_{k+1}^\mu) |C_{N-1}^{(k-1 \leftrightarrow k+1)}\rangle, \quad (10)$$

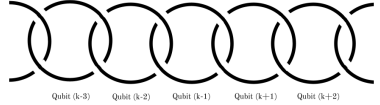
where S denotes the single-qubit phase gate (also called the S gate or $\frac{\pi}{2}$ phase gate, defined by the matrix $S = \text{diag}(1, i) = \begin{pmatrix} 1 & 0 \\ 0 & i \end{pmatrix}$). The operators S_{k-1} and S_{k+1} denote the local phase gates acting on the neighbouring qubits $k - 1$ and $k + 1$. Crucially, the Schmidt Rank (R) across the partition is 2, confirming that the chain remains physically intact.

VI.2. Boundary Phase (End Measurement)

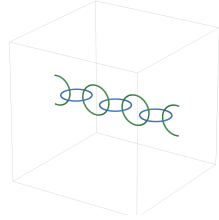
When measuring an endpoint qubit (Q_1), the operation behaves like a *boundary twist*. As shown in APPENDIX C.1, the measurement shortens the chain but imprints a local phase gate onto the new boundary qubit Q_2 . Thus we have

$$|\Psi_{\text{final}}\rangle = S_2^{\pm 1} |C_{N-1}\rangle_{2\dots N}. \quad (11)$$

In the notation $S_2^{\pm 1}$, the superscript ± 1 denotes phase gate or its inverse, depending on the measurement outcome while the subscript 2 indicates which qubit the



(a) Bulk Measurement (2D Schematic)



(b) Bulk Measurement (3D Visualization)

Figure 7: The Bulk Splicing Ambiguity. Measuring a bulk qubit fuses the neighbors $(k - 1, k + 1)$. In this standard 1D topology, the outcome for the Y-basis (Complex Splicing) appears **identical** to the X-basis (Real Splicing). Both result in a single Hopf link. The model is *phase-blind*, failing to show that the Y-basis actually induces a 90° topological twist relative to the X-basis flat frame.

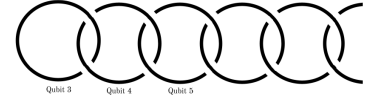
operator acts on. This contrasts with the Z -basis (which simply removes Q_1) and the X -basis (which decouples Q_2).

VII. SUMMARY OF SINGLE-QUBIT MEASUREMENTS

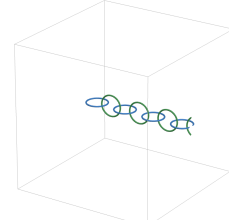
We summarize below (in table I), the exact mathematical results of projective measurements on $|C_N\rangle$ of eq.(4). The following table I condenses the derivations provided in Appendices A , B , and C , detailing the residual state and entanglement properties for end-qubit ($k = 1$) and bulk-qubit ($1 < k < N$) measurements.

VIII. TOPOLOGICAL AMBIGUITY BETWEEN X- AND Y-BASIS MEASUREMENTS

In the standard linear Hopf chain representation (including earlier link based analogies), the topology is characterized solely by binary connectivity i.e two components are either linked or unlinked. Consequently, this representation *does not distinguish* between transverse (X -basis) and lateral (Y -basis) measurements, despite their distinct phase structures. A bulk measurement in the X -basis removes the measured qubit and fuses its neighbours, producing correlations with real amplitudes



(a) End Measurement (2D Schematic)



(b) End Measurement (3D Visualization)

Figure 8: The Boundary Ambiguity. In the standard linear link model, measuring the end qubit (Q_1) is visualized simply as *pruning* the terminal ring. This geometric operation is *indistinguishable* for X and Y measurements. The model fails to capture the physical distinction: that X -measurements typically decouple the next qubit (Q_2), while Y -measurements maintain connectivity but induce a chiral phase twist (S gate) on the boundary.

(± 1) while preserving connectivity. Contrast to this, a Y -basis measurement yields an analogous fusion of neighbouring components but generates intrinsically complex correlations ($\pm i$). In both cases, the resulting topology corresponds to a single Hopf link between the neighbouring components. As a result, the conventional unframed link description is *phase-blind*. It *captures* connectivity changes but *cannot* represent the phase structure introduced by the measurement. This limitation persists for boundary measurements. In the standard link picture, both X - and Y -basis measurements on an end-qubit appear as *identical pruning* operations that remove the terminal component, even though the underlying quantum processes *differ*. X -basis measurements typically propagate logical information along the chain, whereas Y -basis measurements imprint local phase rotations on the neighbouring qubit.

VIII.1. Necessity of a framed description

The origin of this ambiguity lies in the dimensionality of the conventional representation. One-dimensional link diagrams encode connectivity but cannot support internal geometric twist and therefore cannot represent phase information associated with measurement-induced unitary corrections. To obtain a phase sensitive topological description, the link model must be extended to a *framed*

Basis	Target	Outcome	Post-Measurement State	Entanglement Properties
Z	End (Q_1)	$ 0\rangle_1$	$ C_{N-1}\rangle_{2\dots N}$	Chain Shortened ($N \rightarrow N-1$).
	(Comp.)	$ 1\rangle_1$	$Z_2 C_{N-1}\rangle_{2\dots N}$	Chain Shortened + Pauli Z on Q_2 .
Bulk (Q_k)	$ 0\rangle_k$	$ C_L\rangle \otimes C_R\rangle$	Severed ($R=1$). Disconnected.	
	$ 1\rangle_k$	$(Z_{k-1}Z_{k+1})(C_L\rangle \otimes C_R\rangle)$	Severed + Boundary Z corrections.	
X	End (Q_1)	$ +\rangle_1$	$ 0\rangle_2 \otimes C_{N-2}\rangle_{3\dots N}$	Q_2 Decouples. Boundary skips to Q_3 .
	(Trans.)	$ -\rangle_1$	$ 1\rangle_2 \otimes Z_3 C_{N-2}\rangle_{3\dots N}$	Q_2 Decouples. Boundary skips + Z_3 .
Bulk (Q_k)	$ +\rangle_k$	$ C_{N-1}^{(k-1 \leftrightarrow k+1)}\rangle$	Spliced ($R=2$). Real correlations.	
	$ -\rangle_k$	$Z_{k-1} C_{N-1}^{(k-1 \leftrightarrow k+1)}\rangle$	Spliced + Pauli Z on Q_{k-1} .	
Y	End (Q_1)	$ +i\rangle_1$	$S_2 C_{N-1}\rangle_{2\dots N}$	Shortened + Phase Gate S on Q_2 .
	(Lat.)	$ -i\rangle_1$	$S_2^\dagger C_{N-1}\rangle_{2\dots N}$	Shortened + Phase Gate S^\dagger on Q_2 .
Bulk (Q_k)	$ +i\rangle_k$	$(S_{k-1}S_{k+1}) C_{N-1}^{(k-1 \leftrightarrow k+1)}\rangle$	Twisted Splice ($R=2$). Chiral $(+i)$.	
	$ -i\rangle_k$	$(S_{k-1}^\dagger S_{k+1}^\dagger) C_{N-1}^{(k-1 \leftrightarrow k+1)}\rangle$	Twisted Splice. Anti-Chiral $(-i)$.	

Table I: Mathematical summary of single-qubit measurements on the 1D Linear Cluster State. The table explicitly details the post-measurement state for each outcome, highlighting the specific Pauli or Phase corrections induced on the remaining system.

representation in which each component carries an additional geometric degree of freedom corresponding to ribbon orientation. Within this framework, measurement-induced quantum phases are encoded not through connectivity alone but through the framing of the connecting ribbons. In particular, Y -basis measurements correspond to *twisted splicing operations*, where the fused ribbon acquires a chiral twist representing the complex phase $\pm i$. This motivates the framed-ribbon formulation developed in the following section, which provides a unified, phase-sensitive topological representation of single-qubit measurements on linear cluster states.

IX. THE FRAMED RIBBON MODEL: A UNIFIED TOPOLOGICAL FRAMEWORK

To resolve this ambiguity, we introduce a framed ribbon representation, drawing on the mathematical theory of framed knots [28, 34]. In this extended framework, quantum correlations are encoded not only through connectivity but also via geometric twist, with chiral $\pm 90^\circ$ twists corresponding to the phases $\pm i$. (A geometric object is said to be *chiral* if it cannot be superposed onto its mirror image by any combination of rotations and translations. Equivalently, the object possesses a *handedness*, right-handed or left-handed, that distinguishes it from its mirror reflected configuration. In the present framework, the $\pm 90^\circ$ ribbon twists are chiral because right-handed and left-handed twists correspond to physically distinct configurations representing the phases $\pm i$.) This mapping

from quantum phase to geometric torsion parallels the correspondence between quantum evolution and geometric phases [23, 33]. We define the ribbon \mathcal{R} connecting neighbours $k-1$ and $k+1$ by its *Twist Angle* θ , which encodes the relative quantum phase ϕ of the spliced state according to the map $\theta = \phi$. In the APPENDIX D we define the framed ribbon and chirality.

IX.1. The Twist Dictionary

Before analyzing the specific basis measurements, we establish the geometric dictionary of the ribbon.

We consider the ribbon in isolation (qubits removed for clarity), as shown in Fig. 9. To establish the geometric correspondence between ribbon framing and quantum phase, we introduce a twist angle parameter θ that characterizes the relative rotation of a ribbon connecting neighbouring qubits. In the framed ribbon representation, this geometric twist encodes the phase factor associated with the corresponding quantum correlation. The mapping between twist angle and phase is defined as $\theta = \phi$, where ϕ denotes the relative quantum phase.

We distinguish the following canonical configurations.

1. *Flat ribbon* ($\theta = 0^\circ$): The ribbon connects the neighbouring qubits without rotation. This configuration corresponds to the trivial phase factor $+1$ and represents real, positive correlations.

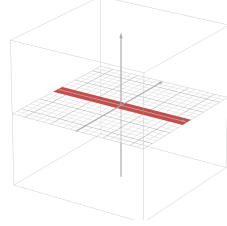
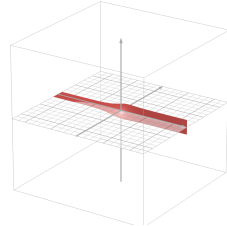
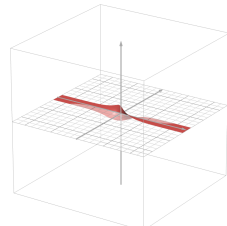
(a) Flat (0°)(b) Chiral (90°)(c) Full Flip (180°)

Figure 9: The Twist Dictionary. (a) Flat ribbon representing quantum phase $+1$. (b) Chiral twist representing quantum phase $\pm i$. (c) Full flip representing quantum phase -1 .

2. *Chiral quarter-twist* ($\theta = \pm 90^\circ$): The ribbon undergoes a quarter rotation, producing a chiral configuration that distinguishes the two possible orientations viz.

- Right-handed twist ($+90^\circ$): corresponds to the phase factor $+i$.
- Left-handed twist (-90°): corresponds to the phase factor $-i$.

3. *Half-twist* ($\theta = 180^\circ$): The ribbon undergoes a half rotation, reversing its orientation. This configuration corresponds to the phase factor -1 , equivalent to the action of a Pauli- Z operator on the associated correlation.

This twist dictionary provides the geometric basis for representing measurement-induced phase transformations within the framed-ribbon model, enabling a unified topological description of both real and complex correlations generated by single-qubit measurements [38].

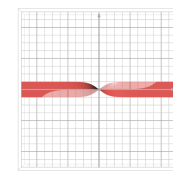
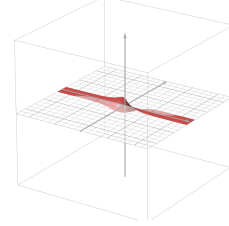


Figure 10: Positive (Right-Handed) Rotation. The ribbon twists clockwise ($+90^\circ$), representing the phase factor $+i$. Note the specific over-crossing structure in both views.

IX.2. Positive and Negative Rotation: Defining Chirality

A critical feature of the Framed Ribbon Model is its ability to distinguish between conjugate complex phases, $+i$ and $-i$, through geometric chirality. Unlike the flat ($\theta = 0^\circ$) or flipped ($\theta = 180^\circ$) ribbons, which are *achiral* (i.e. superposable on their mirror images), the quarter-twist ($\theta = 90^\circ$) *breaks spatial symmetry*. We define the sign of the rotation using the standard Right-Hand Rule along the propagation axis of the cluster.

1. *Positive Rotation (Right-Handed, $+90^\circ$)*: As the ribbon propagates from the qubit Q_{k-1} to the qubit Q_{k+1} , a clockwise rotation of the frame corresponds to a positive phase shift $+i$. Visually, this manifests as the right edge of the ribbon crossing **OVER** the left edge. This specific topology encodes the measurement outcome $|+i\rangle$ (Fig. 10).
2. *Negative Rotation (Left-Handed, -90°)*: A counter-clockwise rotation corresponds to a negative phase shift $-i$. Visually, this manifests as the right edge crossing **UNDER** the left edge. This specific topology encodes the measurement outcome $| -i \rangle$ (Fig. 11).

This geometric encoding of quantum phases through ribbon framing parallels the well-established correspondence between quantum evolution and geometric phases in adiabatic and holonomic quantum computation [23, 24, 33].

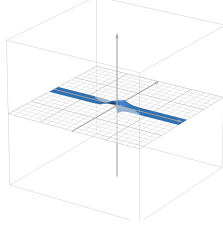


Figure 11: **Negative (Left-Handed) Rotation.** The ribbon twists counter-clockwise (-90°), representing the phase factor $-i$. Note the specific under-crossing structure in both views.

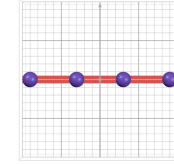


Figure 12: **The Flat Ribbon Chain.** The initial state $|C_N\rangle$ is represented as a linear array of spheres connected by flat, untwisted ribbons ($\theta = 0^\circ$), reflecting the real-valued nature of the initial CZ entanglement.

X. CLUSTER STATE IN THE RIBBON FRAME

X.1. The Initial State in the Ribbon Frame

Before analyzing measurement dynamics, we must define the initial resource state $|C_N\rangle$ of Eq.(4) within this topological framework. Recall that the standard LCS is generated by applying CZ gates to a register of $|+\rangle$ states. The CZ interaction corresponds to the Ising phase factor $(-1)^{x_i x_{i+1}}$. Crucially, this factor is purely real. In our Twist Dictionary, a real correlation corresponds to an untwisted connection. Therefore, we map the initial LCS $|C_N\rangle$ to a *Flat Ribbon Chain*, illustrated in Fig. 12:

- *Spheres (S):* The N qubits are represented as N aligned spheres.
- *Connecting Ribbons (\mathcal{R}):* Each adjacent pair $(i, i+1)$ is connected by a ribbon $\mathcal{R}_{i,i+1}$ initialized with a twist angle $\theta = 0^\circ$.

This *zero-writhe* initialization is the topological dual to the standard graph state definition, where edges represent simple binary connectivity without complex phase. *Zero-writhe* refers to the geometric condition that the ribbons representing entangling links in the initial cluster state carry no intrinsic twist or coiling i.e. the ribbon framing is flat everywhere before any measurement-induced operation. All subsequent measurement-induced twists (chiral $\pm 90^\circ$ or flipped 180°) are defined as deviations from this flat inertial frame.

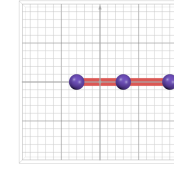
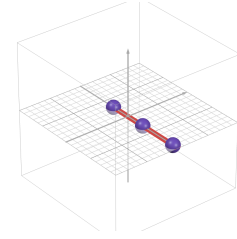


Figure 13: **Z-Basis Pruning (Outcome $|0\rangle_1$).** The measurement removes the first sphere and the ribbon $\mathcal{R}_{1,2}$. The remaining chain starts at Q_2 with no induced twist.



X.2. Case I: Z-Basis (Topological Severance)

As we know the Z -basis measurement is destructive, the ribbon topology is defined by its discontinuity.

X.2.1. Measurement of end-qubit (Q_1)

- *Outcome $|0\rangle_1$ Topology (PRUNING.:)* The first ribbon segment is removed. The chain shortens ($N \rightarrow N - 1$), as shown in Fig. 13. No twist is induced on the remaining bulk.
- *Outcome $|1\rangle_1$ Topology (PRUNING WITH FLIP:)* The

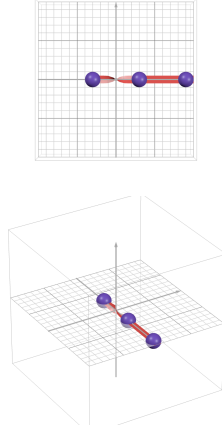


Figure 14: **Z-Basis Pruning with Flip (Outcome $|1\rangle_1$)**. The measurement removes the qubit Q_1 . The resulting Pauli Z correction on the qubit Q_2 manifests as a 180° flip on the *subsequent* ribbon $\mathcal{R}_{2,3}$.

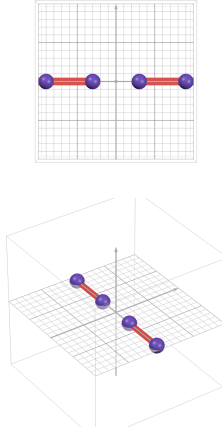


Figure 15: **Z-Basis Severance (Outcome $|0\rangle_k$)**. The central sphere Q_k and its attached ribbons are removed. The chain is physically cut into two disconnected, untwisted segments.

first ribbon is removed. The outcome induces a Pauli Z on the qubit Q_2 . In the ribbon frame, this corresponds to a 180° flip of the next ribbon in the chain (between qubits Q_2 and Q_3), visualized in Fig. 14.

X.2.2. Measurement of bulk-qubit (Q_k)

- *Outcome $|0\rangle_k$ Topology (CLEAN CUT:)* The ribbon at site k is severed. The left and right segments are topologically disconnected ($R = 1$), as depicted in Fig. 15.
- *Outcome $|1\rangle_k$ Topology (CUT WITH BOUNDARY FLIP:)* The ribbon is severed. The outcome applies

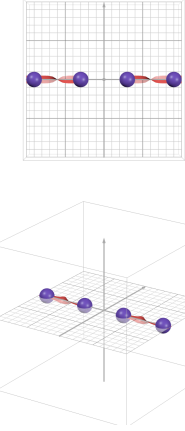


Figure 16: **Severance with Boundary Flips (Outcome $|1\rangle_k$)**. The chain is cut at Q_k . The byproduct operators $Z_{k-1}Z_{k+1}$ induce 180° flips on the ribbons adjacent to the cut ($\mathcal{R}_{k-2,k-1}$ and $\mathcal{R}_{k+1,k+2}$).

Z operators to neighbours Q_{k-1} and Q_{k+1} . This manifests as a 180° flip on the adjacent ribbons connecting them to the rest of the chain, shown in Fig. 16.

X.3. Case II: X-Basis (Real Splicing)

The X -basis measurement preserves connectivity via *Flat* or *Flipped* splicing.

X.3.1. Measurement of end-qubit (Q_1)

- *Outcome $|+\rangle_1$ Topology (SHORTENING:)* The measurement disentangles Q_2 . The active boundary effectively skips to Q_3 , illustrated in Fig. 17. The logic flows forward without twist.
- *Outcome $|-\rangle_1$ Topology (SHORTENING WITH FLIP:)* The boundary skips to Q_3 , but the induced Z operator creates a 180° flip on the new boundary ribbon (Fig. 18).

X.3.2. Measurement of Bulk Qubit (Q_k)

- *Outcome $|+\rangle_k$ Topology FLAT SPLICE ($\theta = 0^\circ$):* Neighbours Q_{k-1} and Q_{k+1} are fused. The ribbon connecting them is perfectly flat (untwisted), representing the correlation $+1$, as shown in Fig. 19.
- *Outcome $|-\rangle_k$ Topology FLIPPED SPLICE ($\theta = 180^\circ$)* Neighbours are fused, but the ribbon undergoes a full 180° rotation (Fig. 20). This topological flip encodes the negative parity correlation -1 .

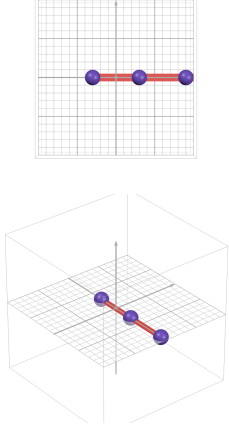


Figure 17: **X-Basis Flat Shortening (Outcome $|+\rangle_1$)**. Q_1 is removed and Q_2 is disentangled. The active boundary skips to Q_3 , with the new boundary ribbon $\mathcal{R}_{3,4}$ remaining flat ($\theta = 0^\circ$).

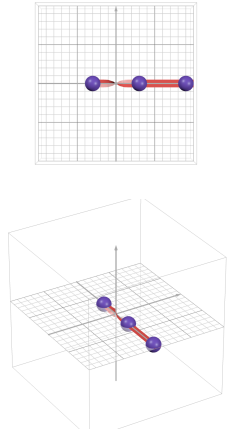


Figure 18: **X-Basis Flipped Shortening (Outcome $|-\rangle_1$)**. The boundary skips to Q_3 . The negative parity outcome induces a Z_3 correction, causing the new boundary ribbon $\mathcal{R}_{3,4}$ to flip 180° .

X.4. Case III: Y-Basis (Chiral Splicing)

The Y -basis measurement embeds complex phase via *Twisted splicing*.

X.4.1. Measurement of end-qubit (Q_1)

- *Outcome $|+i\rangle_1$ Topology RIGHT-HANDED BOUNDARY TWIST*: The chain shortens, but the open end of the ribbon at Q_2 is twisted $+90^\circ$ (Clockwise), as visualized in Fig. 21. This represents the application of the S gate.
- *Outcome $| -i\rangle_1$ Topology LEFT-HANDED BOUNDARY*

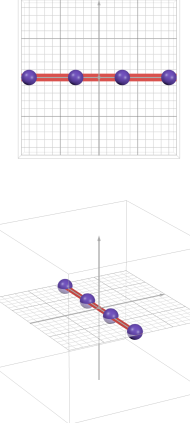


Figure 19: **Flat Splicing (Outcome $|+\rangle_k$) Neighbours** Q_{k-1} and Q_{k+1} are fused. The resulting ribbon is perfectly flat ($\theta = 0^\circ$), indicating positive real correlation $(+1)$.

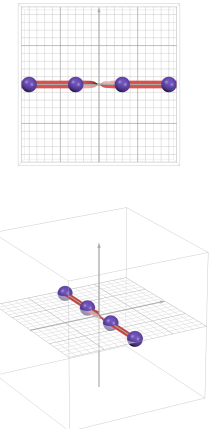


Figure 20: **Flipped Splicing (Outcome $|-\rangle_k$)**. Neighbours are fused, but the ribbon undergoes a 180° flip. This topological inversion corresponds to the negative real correlation (-1) .

TWIST: The chain shortens, and the ribbon at Q_2 is twisted -90° (Counter-Clockwise), shown in Fig. 22. This represents the S^\dagger gate.

X.4.2. Measurement of bulk-qubit (Q_k)

- *Outcome $|+i\rangle_k$ Topology RIGHT-HANDED SPLICE ($\theta = +90^\circ$)*: Neighbours Q_{k-1} and Q_{k+1} are fused. The connecting ribbon has a chiral $+90^\circ$ twist (Right-Over-Left), encoding the phase $+i$ (Fig. 23).
- *Outcome $| -i\rangle_k$ Topology LEFT-HANDED SPLICE ($\theta = -90^\circ$)*: Neighbors are fused. The connecting ribbon has a chiral -90° twist (Right-Under-Left),

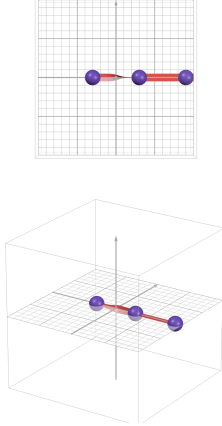


Figure 21: **Right-Handed Boundary Twist (Outcome $|+i\rangle_1$)** The boundary moves to Q_2 . The open end of the ribbon $\mathcal{R}_{2,3}$ acquires a $+90^\circ$ clockwise twist, visualized as the right edge crossing *OVER* the left.

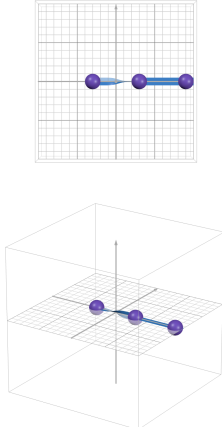


Figure 22: **Left-Handed Boundary Twist (Outcome $| -i\rangle_1$)**. The boundary moves to Q_2 . The ribbon $\mathcal{R}_{2,3}$ acquires a -90° counter-clockwise twist, visualized as the right edge crossing **UNDER** the left.

encoding the phase $-i$, as depicted in Fig. 24.

XI. CONCLUSION

We have established a complete topological classification of single-qubit measurements on linear cluster states. Our analysis reveals three fundamentally distinct measurement-induced transformations, as summarized in Table II.

This classification provides a geometric interpretation of measurement-based quantum computation (MBQC) through the *measurement-cutting correspondence*, which maps local projective measurements to topological

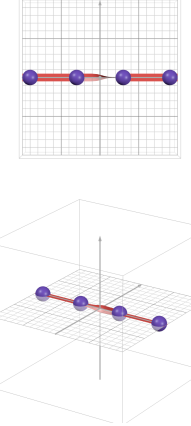


Figure 23: **Right-Handed Twisted Splice (Outcome $|+i\rangle_k$)**. Neighbors Q_{k-1} and Q_{k+1} are fused. The connecting ribbon exhibits a $+90^\circ$ chiral twist, encoding the complex phase $+i$.

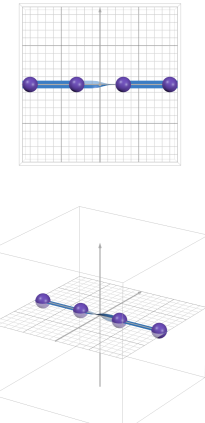


Figure 24: **Left-Handed Twisted Splice (Outcome $| -i\rangle_k$)**. Neighbors are fused with a -90° chiral twist. The change in crossing (Under vs. Over) visually distinguishes this from the $|+i\rangle$ outcome.

surgery operations on a Hopf chain representation of the cluster state.

We have shown that (i) Z -basis measurements act as *topological severance*, physically disconnecting the chain (Schmidt rank $R = 1$) and shortening boundaries without introducing complex phases, (ii) X -basis measurements perform *topological splicing*, preserving connectivity ($R = 2$) through real-valued correlations while actively propagating information along the chain and (iii) Y -basis measurements induce *twisted splicing*, maintaining connectivity ($R = 2$) but imprinting chiral complex phases ($\pm i$) that are invisible in standard link models. The central limitation of conventional topological models is their *phase blindness*: while they

Basis	Topological Operation	Schmidt Rank (Bulk)	Phase Structure	Information Flow
Z	Severance	R=1 (disconnected)	Real (± 1)	Boundary shortening
X	Splicing	R=2 (connected)	Real (± 1)	Active propagation
Y	Twisted Splicing	R=2 (connected)	Complex ($\pm i$)	Phase-modulated flow

Table II: **Synthesis of Measurement Classification.** The triality of measurement operations emerges from our topological analysis, with phase structure distinguishing X from Y measurements despite identical connectivity preservation.

faithfully capture connectivity changes, they cannot distinguish between X and Y basis measurements, which produce identical linking patterns despite fundamentally different phase structures. We resolved this ambiguity by introducing a *framed ribbon model* where quantum phases are encoded as geometric *twists* *flat ribbons* (0°) for real positive correlations, *flipped ribbons* (180°) for real negative correlations, and *chiral twists* ($\pm 90^\circ$) for complex phases $\pm i$. This framing provides unambiguous topological signatures for all measurement outcomes and establishes a unified geometric language for phase-sensitive quantum correlations.

Several promising research directions emerge from this framework such as (a) Generalizing the framed ribbon model to 2D and 3D cluster states [2] may reveal richer topological structures—potentially involving braided ribbons or more complex framed surfaces—associated with multi-qubit measurements and universal MBQC patterns (*Extension to Higher Dimensions*), (b) Incorporating time ordering, classical feedforward, and adaptive measurement strategies into the topological picture could yield fully geometric descriptions of complete quantum circuits, potentially revealing new invariants related to computational depth or complexity (*Dynamic and Adaptive Circuits*), (c) The relationship between ribbon framing, local Clifford operations, and fault-tolerant logical gates suggests potential links with topological error correction [16, 17]. Framed topological invariants might quantify protected quantum information flow or classify fault-tolerant MBQC schemes (*Connections to Topological Quantum Computation*), (iv) Applying this framework to non-stabilizer resources (magic states, hypergraph states) may provide geometric insights into contextuality, quantum advantage, and the role of complex phases in quantum computational supremacy (*Beyond Stabilizer States*) and (v) Developing software tools to visualize measurement sequences using our topological framework could enhance understanding of MBQC dynamics and provide intuitive educational resources (*Experimental Visualization*).

In summary, our work establishes that framed topology provides a natural and physically transparent language

for describing phase-sensitive quantum correlations generated by measurement. By bridging quantum information theory with geometric topology, this approach offers new perspectives on measurement-based quantum computation and suggests that geometric methods may play an increasingly central role in understanding and designing quantum information protocols.

Declaration of competing interest The authors declare that they have no known competing financial interests or personal relationships that could have appeared to influence the work reported in this paper.

Data availability statement No external data is required for this research work.

Appendix A: Z-Basis Measurement on a 1D Cluster State

We present a detailed derivation of projective measurements in the Z basis for a 1D cluster state. End-qubit and bulk-qubit measurements are treated separately. All calculations are carried out using the computational-basis definition of the cluster state with explicit summation over binary variables.

1. Definition of the Cluster State

The N -qubit 1D cluster state is

$$|C_N\rangle = \frac{1}{2^{N/2}} \sum_{x_1, \dots, x_N \in \{0,1\}} (-1)^{\sum_{i=1}^{N-1} x_i x_{i+1}} |x_1 x_2 \dots x_N\rangle, \quad (\text{A1})$$

where all additions in the exponent are understood modulo 2.

The Z -basis eigenstates are

$$|0\rangle, \quad |1\rangle, \quad (\text{A2})$$

with projectors

$$P_0 = |0\rangle\langle 0|, \quad P_1 = |1\rangle\langle 1| \quad (\text{A3})$$

2. Measurement on an end-qubit

We first consider measurement of the end qubit 1 in the Z basis.

a. Initial State and Decomposition

Separate the x_1 -dependent term in the cluster phase:

$$\sum_{i=1}^{N-1} x_i x_{i+1} = x_1 x_2 + \sum_{i=2}^{N-1} x_i x_{i+1}. \quad (\text{A4})$$

Substituting into Eq. (A1),

$$|C_N\rangle = \frac{1}{2^{N/2}} \sum_{x_2, \dots, x_N} (-1)^{\sum_{i=2}^{N-1} x_i x_{i+1}}$$

$$\sum_{x_1=0}^1 (-1)^{x_1 x_2} |x_1\rangle_1 |x_2 \dots x_N\rangle. \quad (\text{A5})$$

b. Outcome $|0\rangle_1$

Applying the projector $\langle 0|_1$ fixes $x_1 = 0$:

$$|\Psi_0\rangle = \langle 0|_1 |C_N\rangle = \frac{1}{2^{N/2}} \sum_{x_2, \dots, x_N} (-1)^{\sum_{i=2}^{N-1} x_i x_{i+1}} |x_2 \dots x_N\rangle. \quad (\text{A6})$$

This is exactly the $(N - 1)$ -qubit cluster state:

$$|\Psi_0\rangle = |C_{N-1}\rangle \quad (\text{A7})$$

c. Outcome $|1\rangle_1$

Applying the projector $\langle 1|_1$ fixes $x_1 = 1$:

$$\begin{aligned} |\Psi_1\rangle &= \langle 1|_1 |C_N\rangle \\ &= \frac{1}{2^{N/2}} \sum_{x_2, \dots, x_N} (-1)^{x_2} (-1)^{\sum_{i=2}^{N-1} x_i x_{i+1}} |x_2 \dots x_N\rangle. \end{aligned} \quad (\text{A8})$$

The factor $(-1)^{x_2}$ is exactly the action of a local Z operator on qubit 2. Thus,

$$|\Psi_1\rangle = Z_2 |C_{N-1}\rangle. \quad (\text{A9})$$

3. Measurement on a bulk-qubit

We now consider measurement of a bulk qubit k with neighbors $k - 1$ and $k + 1$.

a. Initial State and Decomposition

Split the quadratic phase as

$$\sum_{i=1}^{N-1} x_i x_{i+1} = \Phi_{\text{rest}} + x_{k-1} x_k + x_k x_{k+1}, \quad (\text{A10})$$

where Φ_{rest} contains all terms not involving x_k .

Then

$$|C_N\rangle = \frac{1}{2^{N/2}} \sum_{\mathbf{x} \neq k} (-1)^{\Phi_{\text{rest}}} \sum_{x_k=0}^1 (-1)^{x_k(x_{k-1}+x_{k+1})} |x_k\rangle_k |\mathbf{x}_{\neq k}\rangle, \quad (\text{A11})$$

b. Outcome $|0\rangle_k$

Projecting onto $|0\rangle_k$ sets $x_k = 0$:

$$\begin{aligned} |\Psi_0\rangle &= \langle 0|_k |C_N\rangle \\ &= \frac{1}{2^{N/2}} \sum_{\mathbf{x} \neq k} (-1)^{\Phi_{\text{rest}}} |\mathbf{x}_{\neq k}\rangle, \end{aligned} \quad (\text{A12})$$

This corresponds to two disconnected cluster states on the left and right of site k :

$$|\Psi_0\rangle = |C_{k-1}\rangle_L \otimes |C_{N-k}\rangle_R. \quad (\text{A13})$$

c. *Outcome $|1\rangle_k$*

Projecting onto $|1\rangle_k$ sets $x_k = 1$:

$$\begin{aligned} |\Psi_1\rangle &= \langle 1|_k|C_N\rangle \\ &= \frac{1}{2^{N/2}} \sum_{\mathbf{x} \neq k} (-1)^{x_{k-1}+x_{k+1}} (-1)^{\Phi_{\text{rest}}} |\mathbf{x}_{\neq k}\rangle. \end{aligned} \quad (\text{A14})$$

Using

$$(-1)^{x_{k-1}+x_{k+1}} = (-1)^{x_{k-1}} (-1)^{x_{k+1}}, \quad (\text{A15})$$

this factor corresponds to local Z operators acting on both neighbors. Hence,

$$|\Psi_1\rangle = (Z_{k-1} \otimes Z_{k+1}) (|C_{k-1}\rangle_L \otimes |C_{N-k}\rangle_R). \quad (\text{A16})$$

Appendix B: X -Basis Measurement on a 1D Cluster State

We present a detailed derivation of projective measurement in the X basis for a 1D cluster state, treating end-qubit and bulk-qubit measurements separately. All calculations are performed using the computational-basis definition of the cluster state and explicit summation over binary variables.

1. Definition of the Cluster State

The N -qubit 1D cluster state is defined as

$$|C_N\rangle = \frac{1}{2^{N/2}} \sum_{x_1, \dots, x_N \in \{0, 1\}} (-1)^{\sum_{i=1}^{N-1} x_i x_{i+1}} |x_1 x_2 \cdots x_N\rangle \quad (\text{B1})$$

where all additions in the exponent are understood modulo 2.

The X -basis eigenstates are

$$|+\rangle = \frac{|0\rangle + |1\rangle}{\sqrt{2}}, \quad |-\rangle = \frac{|0\rangle - |1\rangle}{\sqrt{2}} \quad (\text{B2})$$

with overlaps

$$\langle \pm | x \rangle = \frac{1}{\sqrt{2}} (\pm 1)^x, \quad x \in \{0, 1\} \quad (\text{B3})$$

2. Measurement on an end-qubit

We first consider measurement of the end qubit 1 in the X basis.

a. Initial State and Decomposition

Separating the x_1 -dependent term in the cluster phase,

$$\sum_{i=1}^{N-1} x_i x_{i+1} = x_1 x_2 + \sum_{i=2}^{N-1} x_i x_{i+1} \quad (\text{B4})$$

Substituting into Eq. (B1),

$$\begin{aligned} |C_N\rangle &= \frac{1}{2^{N/2}} \sum_{x_2, \dots, x_N} (-1)^{\sum_{i=2}^{N-1} x_i x_{i+1}} \\ &\quad \sum_{x_1=0}^1 (-1)^{x_1 x_2} |x_1\rangle_1 |x_2 \cdots x_N\rangle \end{aligned} \quad (\text{B5})$$

b. *Outcome $|+\rangle_1$*

Applying the projector $\langle +|_1$,

$$\begin{aligned} |\Psi_+\rangle &= \langle +|_1 |C_N\rangle \\ &= \frac{1}{2^{(N+1)/2}} \sum_{x_2, \dots, x_N} (-1)^{\sum_{i=2}^{N-1} x_i x_{i+1}} \\ &\quad \sum_{x_1=0}^1 (+1)^{x_1} (-1)^{x_1 x_2} |x_2 \dots x_N\rangle \end{aligned} \quad (\text{B6})$$

Evaluate the inner sum explicitly:

$$\sum_{x_1=0}^1 (+1)^{x_1} (-1)^{x_1 x_2} = \begin{cases} 2, & x_2 = 0 \\ 0, & x_2 = 1 \end{cases} \quad (\text{B7})$$

Thus,

$$|\Psi_+\rangle \propto \sum_{x_3, \dots, x_N} (-1)^{\sum_{i=3}^{N-1} x_i x_{i+1}} |0 x_3 \dots x_N\rangle \quad (\text{B8})$$

After normalization, this is exactly the cluster state $|C_{N-1}\rangle$ on qubits $2, \dots, N$:

$$|\Psi_+\rangle = |C_{N-1}\rangle \quad (\text{B9})$$

c. *Outcome $|-\rangle_1$*

Applying the projector $\langle -|_1$,

$$\begin{aligned} |\Psi_-\rangle &= \langle -|_1 |C_N\rangle \\ &= \frac{1}{2^{(N+1)/2}} \sum_{x_2, \dots, x_N} (-1)^{\sum_{i=2}^{N-1} x_i x_{i+1}} \\ &\quad \sum_{x_1=0}^1 (-1)^{x_1} (-1)^{x_1 x_2} |x_2 \dots x_N\rangle \end{aligned} \quad (\text{B10})$$

The inner sum gives

$$\sum_{x_1=0}^1 (-1)^{x_1} (-1)^{x_1 x_2} = \begin{cases} 0, & x_2 = 0 \\ 2, & x_2 = 1 \end{cases} \quad (\text{B11})$$

Hence,

$$|\Psi_-\rangle \propto \sum_{x_3, \dots, x_N} (-1)^{\sum_{i=3}^{N-1} x_i x_{i+1}} |1 x_3 \dots x_N\rangle \quad (\text{B12})$$

This equals $Z_2 |C_{N-1}\rangle$:

$$|\Psi_-\rangle = Z_2 |C_{N-1}\rangle \quad (\text{B13})$$

3. Measurement on a bulk-qubit

We now measure a bulk qubit k with neighbors $k-1$ and $k+1$.

a. *Initial State and Decomposition*

Split the quadratic phase:

$$\sum_{i=1}^{N-1} x_i x_{i+1} = \Phi_{\text{rest}} + x_{k-1} x_k + x_k x_{k+1} \quad (\text{B14})$$

where Φ_{rest} contains all terms not involving x_k .

Then

$$\begin{aligned} |C_N\rangle &= \frac{1}{2^{N/2}} \sum_{\mathbf{x} \neq k} (-1)^{\Phi_{\text{rest}}} \\ &\quad \sum_{x_k=0}^1 (-1)^{x_k(x_{k-1} \oplus x_{k+1})} |x_k\rangle_k |\mathbf{x} \neq k\rangle \end{aligned} \quad (\text{B15})$$

b. *Outcome $|+\rangle_k$*

Applying $\langle +|_k$,

$$\begin{aligned} |\Psi_+\rangle &= \langle +|_k |C_N\rangle \\ &= \frac{1}{2^{(N+1)/2}} \sum_{\mathbf{x} \neq k} (-1)^{\Phi_{\text{rest}}} \\ &\quad \sum_{x_k=0}^1 (+1)^{x_k} (-1)^{x_k(x_{k-1} \oplus x_{k+1})} |\mathbf{x} \neq k\rangle \end{aligned} \quad (\text{B16})$$

The inner sum evaluates to

$$1 + (-1)^{x_{k-1} \oplus x_{k+1}} \quad (\text{B17})$$

Only configurations with $x_{k-1} = x_{k+1}$ survive, restoring the quadratic term $x_{k-1} x_{k+1}$. After normalization,

$$|\Psi_+\rangle = |C_{N-1}^{(k-1 \leftrightarrow k+1)}\rangle \quad (\text{B18})$$

c. *Outcome $|-\rangle_k$*

Applying $\langle -|_k$,

$$\begin{aligned} |\Psi_-\rangle &= \langle -|_k |C_N\rangle \\ &= \frac{1}{2^{(N+1)/2}} \sum_{\mathbf{x} \neq k} (-1)^{\Phi_{\text{rest}}} \\ &\quad \sum_{x_k=0}^1 (-1)^{x_k} (-1)^{x_k(x_{k-1} \oplus x_{k+1})} |\mathbf{x} \neq k\rangle \end{aligned} \quad (\text{B19})$$

The inner sum gives

$$1 - (-1)^{x_{k-1} \oplus x_{k+1}} \quad (\text{B20})$$

This introduces a relative minus sign equivalent to a local Z operator on either neighbor. Choosing qubit $k-1$,

$$|\Psi_-\rangle = Z_{k-1} |C_{N-1}^{(k-1 \leftrightarrow k+1)}\rangle \quad (\text{B21})$$

Appendix C: Y -Basis Measurement on a 1D Cluster State

We present a detailed derivation of projective measurement in the Y basis for a 1D cluster state, treating end-qubit and bulk-qubit measurements separately. All calculations use the computational-basis definition of the cluster state and explicit summation over binary variables.

1. Definition of the Cluster State

The N -qubit 1D cluster state is

$$|C_N\rangle = \frac{1}{2^{N/2}} \sum_{x_1, \dots, x_N \in \{0,1\}} (-1)^{\sum_{i=1}^{N-1} x_i x_{i+1}} |x_1 x_2 \dots x_N\rangle, \quad (\text{C1})$$

where all sums in the exponent are taken modulo 2.

The Y -basis eigenstates are

$$|y_{\pm}\rangle = \frac{|0\rangle \pm i|1\rangle}{\sqrt{2}} \quad (\text{C2})$$

with overlaps

$$\langle y_{\pm}|x\rangle = \frac{1}{\sqrt{2}} (\pm i)^x, \quad x \in \{0, 1\} \quad (\text{C3})$$

2. Measurement on an end-qubit

We first consider measurement of the end qubit 1 in the Y basis.

a. Initial State and Decomposition

Separating the x_1 -dependent term,

$$\sum_{i=1}^{N-1} x_i x_{i+1} = x_1 x_2 + \sum_{i=2}^{N-1} x_i x_{i+1} \quad (\text{C4})$$

Thus,

$$|C_N\rangle = \frac{1}{2^{N/2}} \sum_{x_2, \dots, x_N} (-1)^{\sum_{i=2}^{N-1} x_i x_{i+1}} \sum_{x_1=0}^1 (-1)^{x_1 x_2} |x_1\rangle_1 |x_2 \dots x_N\rangle \quad (\text{C5})$$

b. Outcome $|y_+\rangle_1$

Applying the projector $\langle y_+|_1$,

$$\begin{aligned} |\Psi_+\rangle &= \langle y_+|_1 |C_N\rangle \\ &= \frac{1}{2^{(N+1)/2}} \sum_{x_2, \dots, x_N} (-1)^{\sum_{i=2}^{N-1} x_i x_{i+1}} \sum_{x_1=0}^1 (i)^{x_1} (-1)^{x_1 x_2} |x_2 \dots x_N\rangle \end{aligned} \quad (\text{C6})$$

The inner sum evaluates to

$$\sum_{x_1=0}^1 i^{x_1} (-1)^{x_1 x_2} = \begin{cases} 1+i, & x_2 = 0 \\ 1-i, & x_2 = 1 \end{cases} \quad (\text{C7})$$

Factoring out $\sqrt{2}e^{i\pi/4}$ and renormalizing, this induces a local S gate on qubit 2. Hence,

$$|\Psi_+\rangle = S_2 |C_{N-1}\rangle \quad (\text{C8})$$

c. Outcome $|y_-\rangle_1$

Applying the projector $\langle y_-|_1$,

$$\begin{aligned} |\Psi_-\rangle &= \langle y_-|_1 |C_N\rangle \\ &= \frac{1}{2^{(N+1)/2}} \sum_{x_2, \dots, x_N} (-1)^{\sum_{i=2}^{N-1} x_i x_{i+1}} \sum_{x_1=0}^1 (-i)^{x_1} (-1)^{x_1 x_2} |x_2 \dots x_N\rangle \end{aligned} \quad (\text{C9})$$

The inner sum gives

$$\sum_{x_1=0}^1 (-i)^{x_1} (-1)^{x_1 x_2} = \begin{cases} 1-i, & x_2 = 0 \\ 1+i, & x_2 = 1 \end{cases} \quad (\text{C10})$$

After normalization, this corresponds to an S^\dagger gate on qubit 2:

$$|\Psi_-\rangle = S_2^\dagger |C_{N-1}\rangle \quad (\text{C11})$$

3. Measurement on a bulk-qubit

We now consider measurement of a bulk qubit k with neighbors $k-1$ and $k+1$.

a. Initial State and Decomposition

Split the quadratic phase:

$$\sum_{i=1}^{N-1} x_i x_{i+1} = \Phi_{\text{rest}} + x_{k-1} x_k + x_k x_{k+1} \quad (\text{C12})$$

where Φ_{rest} excludes all terms involving x_k .

Then

$$|C_N\rangle = \frac{1}{2^{N/2}} \sum_{\mathbf{x} \neq k} (-1)^{\Phi_{\text{rest}}} \sum_{x_k=0}^1 (-1)^{x_k(x_{k-1} \oplus x_{k+1})} |x_k\rangle_k |\mathbf{x} \neq k\rangle \quad (\text{C13})$$

b. *Outcome* $|y_+\rangle_k$

Applying $\langle y_+|_k$,

$$\begin{aligned} |\Psi_+\rangle &= \langle y_+|_k |C_N\rangle \\ &= \frac{1}{2^{(N+1)/2}} \sum_{\mathbf{x} \neq k} (-1)^{\Phi_{\text{rest}}} \\ &\quad \sum_{x_k=0}^1 (i)^{x_k} (-1)^{x_k(x_{k-1} \oplus x_{k+1})} |\mathbf{x} \neq k\rangle \end{aligned} \quad (\text{C14})$$

The inner sum evaluates to

$$1 + i(-1)^{x_{k-1} \oplus x_{k+1}} \quad (\text{C15})$$

Using

$$1 + i(-1)^a = \sqrt{2}e^{i\pi/4}i^a$$

this induces local S gates on both neighbors and restores the quadratic term $x_{k-1}x_{k+1}$.

After normalization,

$$|\Psi_+\rangle = (S_{k-1} \otimes S_{k+1}) |C_{N-1}^{(k-1 \leftrightarrow k+1)}\rangle \quad (\text{C16})$$

c. *Outcome* $|y_-\rangle_k$

Applying $\langle y_-|_k$,

$$\begin{aligned} |\Psi_-\rangle &= \langle y_-|_k |C_N\rangle \\ &= \frac{1}{2^{(N+1)/2}} \sum_{\mathbf{x} \neq k} (-1)^{\Phi_{\text{rest}}} \sum_{x_k=0}^1 (-i)^{x_k} (-1)^{x_k(x_{k-1} \oplus x_{k+1})} |\mathbf{x} \neq k\rangle \end{aligned} \quad (\text{C17})$$

The inner sum gives

$$1 - i(-1)^{x_{k-1} \oplus x_{k+1}}. \quad (\text{C18})$$

This produces the inverse local phases, corresponding to S^\dagger gates:

$$|\Psi_-\rangle = (S_{k-1}^\dagger \otimes S_{k+1}^\dagger) |C_{N-1}^{(k-1 \leftrightarrow k+1)}\rangle \quad (\text{C19})$$

Appendix D: Framed ribbon and chirality

A framed ribbon \mathcal{R}_{ij} connecting qubits Q_i and Q_j is an oriented, embedded strip $I \times [-\epsilon, \epsilon]$ in \mathbb{R}^3 (Euclidean 3D space). Here I parametrizes the core curve from Q_i and Q_j and the interval $[-\epsilon, \epsilon]$ fibers define the framing, (a continuous choice of normal direction along the core). The framing is equivalently specified by a unit normal vector field $n(s)$ along the core curve $\gamma(s)$, $s \in [0, 1]$. The ribbon's two edges are $\gamma(s) \pm \epsilon n(s)$. The twist angle $\theta \in \mathbb{R}$ is defined as the total accumulated rotation of the framing vector $n(s)$ about the tangent direction $t(s)$ as the ribbon is traversed from Q_i to Q_j . For a ribbon lying in a plane without intrinsic torsion, θ is simply the net rotation angle of the ribbon's cross-section. In this work we have considered only discrete, geometrically stabilized framing corresponding to measurement outcomes $\theta \in \{0^\circ, \pm 90^\circ, 180^\circ\} (\text{mod } 360^\circ)$. These are not topological invariants (as they are not preserved under all continuous deformations), but rather geometric labels that are operationally fixed by the quantum measurement protocol. This quantization of twist reflects the discrete nature of measurement outcomes in quantum mechanics. The chirality of a 90° twist is defined with respect to a fixed orientation of cluster chain (from left to right). A right handed $+90^\circ \text{irc}$ twist corresponds to the right edge of the ribbon crossing over the left edge when viewed from above; a left handed -90°irc twist corresponds to the right edge crossing under the left edge.

[1] R. Raussendorf and H. J. Briegel, Phys. Rev. Lett. 86, 5188 (2001), [doi:10.1103/PhysRevLett.86.5188](https://doi.org/10.1103/PhysRevLett.86.5188).

[2] R. Raussendorf, D. E. Browne, and H. J. Briegel, Phys. Rev. A 68, 022312 (2003), [doi:10.1103/PhysRevA.68.022312](https://doi.org/10.1103/PhysRevA.68.022312).

[3] M. Hein et al., Phys. Rev. A 69, 062311 (2004), [doi:10.1103/PhysRevA.69.062311](https://doi.org/10.1103/PhysRevA.69.062311).

[4] M. A. Nielsen, Rep. Math. Phys. 57, 147 (2006), [doi:10.1016/S0034-4877\(06\)80014-5](https://doi.org/10.1016/S0034-4877(06)80014-5).

[5] V. Danos, E. Kashefi, and P. Panangaden, J. ACM 54, 8 (2007), [doi:10.1145/1219092.1219096](https://doi.org/10.1145/1219092.1219096).

- [6] D. E. Browne and T. Rudolph, Phys. Rev. Lett. 95, 010501 (2005), [doi:10.1103/PhysRevLett.95.010501](https://doi.org/10.1103/PhysRevLett.95.010501).
- [7] E. Knill, R. Laflamme, and G. J. Milburn, Nature 409, 46 (2001), [10.1038/35051009](https://doi.org/10.1038/35051009).
- [8] P. Walther, K. J. Resch, T. Rudolph, E. Schenck, H. Weinfurter, V. Vedral, M. Aspelmeyer, and A. Zeilinger, Nature 434, 169 (2005), [doi:10.1038/nature03347](https://doi.org/10.1038/nature03347).
- [9] M. Hein, W. Dür, J. Eisert, R. Raussendorf, M. Van den Nest, and H. J. Briegel, arXiv:quant-ph/0602096, [doi:10.48550/arXiv.quant-ph/0602096](https://doi.org/10.48550/arXiv.quant-ph/0602096).
- [10] M. Van den Nest, J. Dehaene, and B. De Moor, Phys. Rev. A 69, 022316 (2004), [doi:10.1103/PhysRevA.69.022316](https://doi.org/10.1103/PhysRevA.69.022316).
- [11] D. Schlingemann, arXiv:quant-ph/0111080, [doi:10.48550/arXiv.quant-ph/0111080](https://doi.org/10.48550/arXiv.quant-ph/0111080).
- [12] P. Walther et al., Nature 434, 169 (2005), [doi:10.1038/nature03347](https://doi.org/10.1038/nature03347).
- [13] R. Prevedel et al. Nature 445, 65 (2007), [10.1038/nature05346](https://doi.org/10.1038/nature05346).
- [14] D. Gottesman, arXiv:quant-ph/9807006 (1998), [doi:10.48550/arXiv.quant-ph/9807006](https://doi.org/10.48550/arXiv.quant-ph/9807006).
- [15] V. Danos and E. Kashefi, Phys. Rev. A 74, 052310 (2006), [doi:10.1103/PhysRevA.74.052310](https://doi.org/10.1103/PhysRevA.74.052310).
- [16] A. Kitaev, Ann. Phys. (N.Y.) 303, 2 (2003), [doi:10.1016/S0003-4916\(02\)00018-0](https://doi.org/10.1016/S0003-4916(02)00018-0).
- [17] C. Nayak, S. H. Simon, A. Stern, M. Freedman, and S. Das Sarma, Rev. Mod. Phys. 80, 1083 (2008), [doi:10.1103/RevModPhys.80.1083](https://doi.org/10.1103/RevModPhys.80.1083).
- [18] R. W. Ogburn and J. Preskill, Quant. Compt. Quant. Comm., pp 341 - 356, (1999), [10.1007/3-540-49208-9-31](https://doi.org/10.1007/3-540-49208-9-31).
- [19] E. Witten, Commun. Math. Phys. 121, 351 (1989), [doi:10.1007/BF01217730](https://doi.org/10.1007/BF01217730).
- [20] X.-G. Wen, Int. Jour. Mod. Phys. B 4, 239 (1990), [doi:10.1142/S0217979290000139](https://doi.org/10.1142/S0217979290000139).
- [21] X.-G. Wen, Phys. Rev. B 65, 165113 (2002), [doi:10.1103/PhysRevB.65.165113](https://doi.org/10.1103/PhysRevB.65.165113).
- [22] M. Z. Hasan and C. L. Kane, Rev. Mod. Phys. 82, 3045 (2010), [doi:10.1103/RevModPhys.82.3045](https://doi.org/10.1103/RevModPhys.82.3045).
- [23] M. V. Berry, Proc. R. Soc. A. 392, 45 (1984), [doi:10.1098/rspa.1984.0023](https://doi.org/10.1098/rspa.1984.0023).
- [24] P. Zanardi and M. Rasetti, Phys. Lett. A. 264, 94 (1999), [doi:10.1016/S0375-9601\(99\)00803-8](https://doi.org/10.1016/S0375-9601(99)00803-8).
- [25] J. C. Budich and E. Ardonne, Phys. Rev. B., 88, 075419 (2013), [doi:10.1103/PhysRevB.88.075419](https://doi.org/10.1103/PhysRevB.88.075419).
- [26] S. Vijay, J. Haah and L. Fu, Phys. Rev. B 94, 235157 (2016), [10.1103/PhysRevB.94.235157](https://doi.org/10.1103/PhysRevB.94.235157).
- [27] P. K. Aravind, in *Potentiality, Entanglement and Passion-at-a-Distance* (Springer, 1997), [doi:10.1007/978-94-017-2732-7-4](https://doi.org/10.1007/978-94-017-2732-7-4).
- [28] L.H. Kauffman, *Knots and Physics*, Vol.1, World Scientific, ISBN: 978-981-02-0343-6.
- [29] S. Bhattacharyya and S. Roy., arXiv:quant-ph/2509.05972, [doi:10.48550/arXiv.2509.05972](https://doi.org/10.48550/arXiv.2509.05972).
- [30] S. Bhattacharyya and S. Roy., arXiv:quant-ph/2512.12704, [doi:10.48550/arXiv.2512.12704](https://doi.org/10.48550/arXiv.2512.12704).
- [31] B. Coecke and R. Duncan, New. Jour. of Phys., 13, 043016 (2011), [doi:10.1088/1367-2630/13/4/043016](https://doi.org/10.1088/1367-2630/13/4/043016).
- [32] B. Coecke and A. Kissinger, *Picturing Quantum Process*, Cambridge University Press, ISBN: 9781316219317, [doi:10.1017/9781316219317](https://doi.org/10.1017/9781316219317).
- [33] Y. Aharonov and J. Anandan, Phys. Rev. Lett. 58(16), (1987), [doi:10.1103/PhysRevLett.58.1593](https://doi.org/10.1103/PhysRevLett.58.1593)
- [34] C.C.Adams, *The Knot Book: An Elementary Introduction to the Mathematical Theory of Knots*, American Mathematical Society, (2004), ISBN: 978-0-8218-3678-1.
- [35] M.A. Nielsen and I.L. Chuang, *Quantum Computation and Quantum Information*, Cambridge University Press, (2010), ISBN: 978-1-107-00217-3.
- [36] A. Peres, *Quantum Theory: Concepts and Methods*, Kluwer Academic Publishers, (1995), ISBN: 0-7923-2549-4.
- [37] D. Schlingemann, Quant. Inf. Comp., 2(4), (2002), arXiv:quant-ph/0111080, [doi:10.48550/arXiv.quant-ph/0111080](https://doi.org/10.48550/arXiv.quant-ph/0111080).
- [38] D. Rolfsen, *Knots and Links*, 346 (2003), Am. Math. Soc.